Research Square

Preprints are preliminary reports that have not undergone peer review.
They should not be considered conclusive, used to inform clinical practice,
or referenced by the media as validated information.

Cu-Doped Intercalation-Engineered 2D ZIF-8/alk-MXene Heterostructure: A High-Performance Synergistic Adsorbent for Efficient Tetracycline Removal from Wastewater

Handong Leng
Panjin Institute of Industrial Technology, Dalian University of Technology
Xingyu Yang
Panjin Institute of Industrial Technology, Dalian University of Technology
Xu Liu
Panjin Institute of Industrial Technology, Dalian University of Technology
Yingying Zuo
Panjin Institute of Industrial Technology, Dalian University of Technology
Yuhua Gao
Hebei Academy of Sciences
Hanwen Cui
Panjin Institute of Industrial Technology, Dalian University of Technology
Ziyan Wang
Panjin Institute of Industrial Technology, Dalian University of Technology
Penghui Wu
Panjin Institute of Industrial Technology, Dalian University of Technology
Boxing An
Panjin Institute of Industrial Technology, Dalian University of Technology
Zhengqi Liang
Panjin Institute of Industrial Technology, Dalian University of Technology
Hai Liang
Yingkou Institute of Technology
Kangjun Wang
Shenyang University of Chemical Technology
Yushan Li
liyushan@dlut.edu.cn

Panjin Institute of Industrial Technology, Dalian University of Technology

Research Article

Keywords: Cu-ZIF-8/alk-MXene, tetracycline, adsorption, water treatment

Posted Date: November 12th, 2026

DOI: https://doi.org/10.21203/rs.3.rs-11395445/v1

License: This work is licensed under a Creative Commons Attribution 4.0 International License.
Read Full License

Additional Declarations: No competing interests reported.

Cu-Doped Intercalation-Engineered 2D ZIF-8/alk-MXene Heterostructure: A High-Performance Synergistic Adsorbent for Efficient Tetracycline Removal from Wastewater

Handong Leng [a,b,1], Xingyu Yang [a,b,1], Xu Liu[a*], Yingying Zuo[a], Yuhua Gao[d], Hanwen Cui[a b], Ziyan Wang[a b], Penghui Wu[a b], Boxing An[a], Zhengqi Liang[a], Hai Liang[c], Kangjun Wang[b], Yushan Li[a*]

[a] Liaoning Key Laboratory of Chemical Additive Synthesis and Separation, Panjin Institute of Industrial Technology, Dalian University of Technology, Panjin 124221, Liaoning, China.

[b] School of Chemical Engineering, Shenyang University of Chemical Technology, Shenyang 110142, Liaoning, China.

[c] College of Chemistry and Environmental Engineering, Yingkou Institute of Technology, Yingkou 115014, Liaoning, China.

[d] Institute of Energy Resources, Hebei Academy of Sciences, Shijiazhuang 050081, Hebei, China

HIGHLIGHTS

1. A novel Cu-ZIF-8/alk-MXene composite adsorbent is synthesized via in-situ growth.
2. The maximum TC adsorption capacity of Cu-ZIF-8/alk-MXene reaches 1631.1 $mg \cdot g^{-1}$.
3. The composite removes TC via electrostatic attraction, metal coordination and H-bonding.
3. The composite synergistically removes tetracycline (TC) through multiple adsorption mechanisms, including electrostatic attraction, metal coordination, and hydrogen bonding.
4. Cu-ZIF-8/alk-MXene shows stable cycling performance, retaining 1283 $mg \cdot g^{-1}$ after 5 cycles.

[1] The first two authors contribute equally to this paper.

*Corresponding authors.

30 E-mail addresses: xu_liu@dlut.edu.cn (Xu Liu), liyushan@dlut.edu.cn (Yushan Li).
31

ABSTRACT

The safe disposal of high-concentration antibiotic wastewater from medical, livestock and aquaculture sectors is critical to ecological security and public health. Herein, a Cu-doped ZIF-8/alk-MXene heterostructure with a well-defined intercalation structure and ultrahigh adsorption capacity for tetracycline in aquaculture wastewater was rationally fabricated via in-situ growth and post-modification. This heterostructured material (Cu-ZIF-8/alk-MXene) was fabricated via in-situ growth of two-dimensional ZIF-8 nanosheets within the intercalated structure of alkalized MXene (alk-MXene) followed by Cu doping, which synergized the electron-metal-support interactions (EMSI) induced by Cu dopants and the inherent structural merits of alk-MXene. Impressively, the Cu-ZIF-8/alk-MXene adsorbent achieves a remarkably boosted TC adsorption capacity in wastewater through the synergy of electrostatic attraction, metal coordination and π-π interaction. The Pseudo-second-order kinetic and Langmuir isotherm fitting further verify that the adsorption process is mainly controlled by chemical adsorption and follows a monolayer adsorption pattern. The composite delivers a Langmuir maximum TC adsorption capacity of 1631.1 $mg \cdot g^{-1}$, with stable performance across pH 4-10 and initial TC concentrations of 10-200 $mg \cdot L^{-1}$. It also shows excellent reusability: after five consecutive adsorption-desorption cycles, the adsorbent retains approximately 1283 $mg \cdot g^{-1}$ of TC uptake, corresponding to ~78.7% of its initial capacity, and exhibits strong anti-interference ability against coexisting ions in complex water matrices. DFT calculations further verify that the synergistic TC adsorption arises from the combined effects of metal coordination, electrostatic attraction and π-π interaction. This work demonstrates the great application potential of

the as-designed heterostructure for practical tetracycline-contaminated water remediation.

Keywords: Cu-ZIF-8/alk-MXene; tetracycline; adsorption; water treatment

1. Introduction

Antibiotic residues released from medical, livestock and aquaculture activities have become persistent contaminants in aquatic systems [1, 2]. Tetracycline (TC) is of particular concern because its extensive use, limited biodegradability, and retained biological activity favor long-term accumulation and may threaten both ecosystem functions and human health [3, 4]. Therefore, the efficient removal of TC from water remains a critical challenge in wastewater treatment. Among existing wastewater treatment technologies, biological degradation methods are limited in efficiency due to the influence of antibiotic resistance; advanced oxidation technologies, while achieving thorough degradation, are costly and prone to generating byproducts; and membrane separation technologies face challenges related to membrane fouling and high maintenance costs [5, 6]. In contrast, adsorption methods, due to their simplicity, low cost, and environmental friendliness, have emerged as the most promising solution [7]. Consequently, the development of adsorbents that combine high adsorption uptake, excellent selectivity, recyclability, and environmental stability for the efficient removal of TC from water has become one of the key research priorities in the field of

environmental materials [8, 9].

Layered MXenes are attractive supports for contaminant capture because their surfaces contain abundant -OH, -O, and -F terminations and their gallery spacing can be adjusted to regulate molecular transport [10, 11]. MXene possesses a large specific surface area, and its interlayer channels provide efficient diffusion and adsorption pathways for pollutants. However, in practical applications, MXene materials face challenges such as susceptibility to oxidation and interlayer stacking, which limit their long-term stability and adsorption efficiency [12, 13]. Alkali treatment can effectively widen the interlayer spacing of MXene to 0.9-1.2 nm and enhance its oxidation resistance. However, further functionalization remains key to improving adsorption performance [14, 15]. Metal-organic frameworks provide a complementary platform. In particular, zeolitic imidazolate frameworks combine high porosity, adjustable pore environments, and good chemical robustness [16-18]. ZIF-8 is a typical ZIF material that is easy to synthesize and structurally stable. However, its adsorption selectivity for polar pollutants remains limited [19, 20]. Metal doping (e.g., with Cu^{2+}) can effectively modulate the electronic structure and surface properties of ZIF-8. The introduction of Cu^{2+} provides additional coordination sites, significantly enhancing the adsorption uptake for TC pollutants [21, 22]. Instead, when ZIF nanocrystals are integrated with layered MXene, interparticle voids, expanded MXene galleries, external/defect sites, and interfacial functional groups can jointly create hierarchical adsorption domains [23-27]. Wang et al. reported that the adsorption uptake of the alk-MXene/ZIF adsorbent for TC reached 1053.3 $mg \cdot g^{-1}$, revealing the role of its intercalation structure in

enhancing stability [28]. Zhu et al. demonstrated that the composite of Cu and ZIF-8 achieved efficient adsorption and recyclability of TC, with the adsorption uptake remaining at over 85% of the initial value after five cycles [29]. Although ZIF/MXene composites have shown great potential for antibiotic adsorption, several key issues remain unresolved. Pristine MXene possesses a two-dimensional layered structure and abundant surface functional groups, but its practical adsorption performance is restricted by layer restacking and structural instability. ZIF-8 has a stable porous framework; however, its affinity toward polar antibiotic molecules such as tetracycline is still limited because of insufficient specific binding sites. Therefore, simply combining MXene with ZIF-8 is not sufficient to fully improve adsorption performance. A rational interfacial design is required to simultaneously enhance mass transfer, expose active sites, and strengthen adsorbent-TC interactions.

To address these limitations, Cu-ZIF-8/alk-MXene was designed as an interface-coupled composite adsorbent in this work. Alk-MXene was selected as the layered support to enlarge interlayer spacing, suppress restacking, and provide Ti-OH-related surface functional groups. At the same time, Cu-doped ZIF-8 was introduced to enrich Zn^{2+}/Cu^{2+} coordination sites and construct porous adsorption domains. This structure is expected to promote TC diffusion, improve active-site accessibility, and enhance the synergistic adsorption effects of metal coordination, hydrogen bonding, and electrostatic attraction. More importantly, this study focuses not only on improving adsorption uptake but also on clarifying the relationship among interfacial structure regulation, multi-site adsorption mechanisms, and adsorption stability under complex

aqueous conditions. This study comprehensively employed scanning electron microscopy (SEM) to observe microstructures, X-ray diffraction (XRD) to verify crystal structures and interlayer spacings, BET analysis to characterize pore properties, Changes in surface chemical functionalities were identified by Fourier transform infrared spectroscopy (FTIR). and the elemental distribution and surface chemical states were examined by X-ray photoelectron spectroscopy (XPS). The study systematically investigated the ultra-high adsorption uptake of the synthesized composite material toward tetracycline in water. The effects of experimental factors such as coexisting ions, pH, and temperature on the adsorbent's adsorption performance were discussed. Concurrently, density functional theory (DFT) calculations were employed to provide an in-depth analysis at the atomic and molecular levels of the synergistic adsorption mechanism involving electrostatic attraction, metal coordination, and hydrogen bonding. This study offers new insights for the design of Cu-ZIF-8/alk-MXene composite adsorbents, lays a theoretical and technical foundation for the development of highly efficient antibiotic adsorption materials, and holds significant implications for addressing water pollution and safeguarding ecological and human health.

2.Experimental

2.1 Materials and methods

Chemical reagents, characterization techniques and part of experimental methods referred in this work are described in supplementary material（Text 2 Experimental）.

2.2 Synthesis of Cu-ZIF-8/alk-MXene

Add 0.1 g of alk-MXene to 50 mL of a solution containing 1.3623 g of $ZnCl_2$. Then, stir under a magnetic stirrer for 1 h, and dissolve 3.284 g of 2-methylimidazole(2-MIM) in 50 mL of deionized water, resulting in a Zn(II):2-MIM molar ratio of 1:4. The two solutions were mixed and magnetically stirred at 85 °C for 12 h. The mixture was then centrifuged and washed several times with deionized water, and the resulting precipitate was freeze-dried for 48 h. This yielded the ZIF-8/alk-MXene composite. Next, 0.48 g of the material was added to 40 mL of a solution containing 0.12 g of $Cu(NO_3)_2 \cdot 3H_2O$ and magnetically stirred at 25 °C for 1 h. This post-treatment introduced Cu^{2+} ions to enhance the composite's coordination adsorption capacity for TC. The mixture was then centrifuged and washed several times, followed by freeze-drying for 24 h, yielding the Cu-ZIF-8/alk-MXene composite.

2.3 DFT calculations

The molecular-level interactions between TC and Cu-ZIF-8/alk-MXene were examined through DFT calculations performed using the $DMol^3$ program within the Materials Studio platform. The Perdew-Burke-Ernzerhof (PBE) coupling functional under the Generalized Gradient Approximation (GGA) was selected, and the molecular electrostatic potential (MEP) and charge density distributions and analyzed to identify the patterns of charge distribution changes before and after adsorption.

3.Results and Discussion

3.1 Characterization

3.1.1SEM

The microstructure and morphological changes of the MXene、alk-MXene、ZIF-8 and Cu-ZIF-8/alk-MXene composite were examined using a scanning electron microscope (SEM). As shown in Fig. 1(A-C), the MXene material exhibits a typical two-dimensional layered structure, with no obvious pores or gaps visible on its surface. This is due to stacking effects caused by interlayer interactions within the MXene, which limit its adsorption performance [30, 31]. As shown in Fig. 1(D-F), after alkaline etching, the interlayer spacing of the MXene material increases, forming a multi-layer stacked structure [32]. The microscopic morphology of 2D ZIF-8 nanosheets presented in Fig. 1G shows randomly oriented stacked sheet-like cluster geometry, which forms a multi-layered surface topography with abundant large interlayer voids, and this structure is consistent with the reports of previous studies [33, 34]. Further observation in Fig. 1(H-I) revealed that the two-dimensional lamellar structure of 2D ZF-8 was loaded onto the surface of MXene, forming a multi-level three-dimensional composite material Cu-ZF-8/alk-MXene. The above structure not only retains the metal frame of ZIF-8, but also enhances the surface roughness and inter-layer channels through layered stacking, and increases the specific surface area of the material through multi-dimensional integration [35]. Elemental mapping analysis Fig. 1(J-O) further indicates that characteristic elements such as C, N, O, F, Cu, and Ti exhibit uniform spatial distribution within the composite material. Combining the SEM and EDS results, the

successful synthesis of the Cu-ZIF-8/alk-MXene composite is demonstrated. Inductively coupled plasma (ICP) measurements, as presented in supporting information Table S1, reveal that the combined content of Zn and Cu reaches 22.39%, with Zn accounting for 15.44% and Cu for 6.95%. This confirms that the composite possesses a substantial number of active adsorption sites.

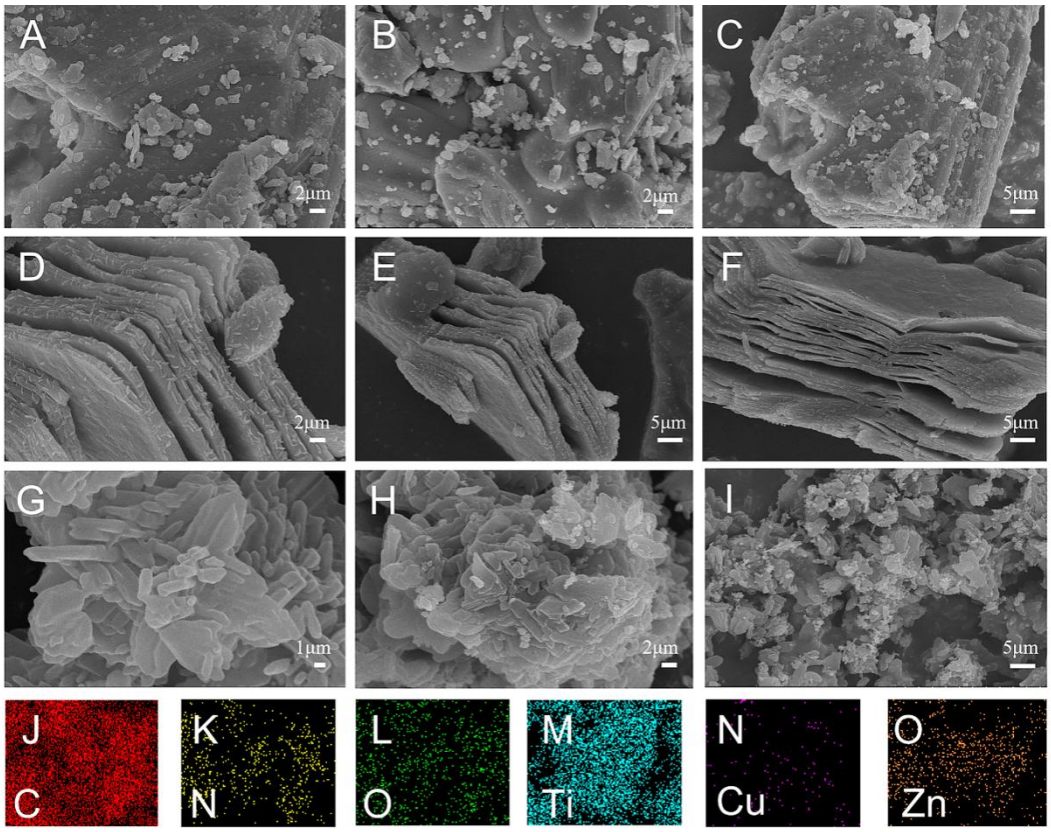


Fig. 1. Morphology and elemental distribution of the as-prepared samples. (A-C) MXene materials; (D-F) alk-MXene; (G) ZIF-8, (H-I) Cu-ZIF-8/alk-MXene composites; (J-O) Cu-ZIF-8/alk-MXene elemental mapping.

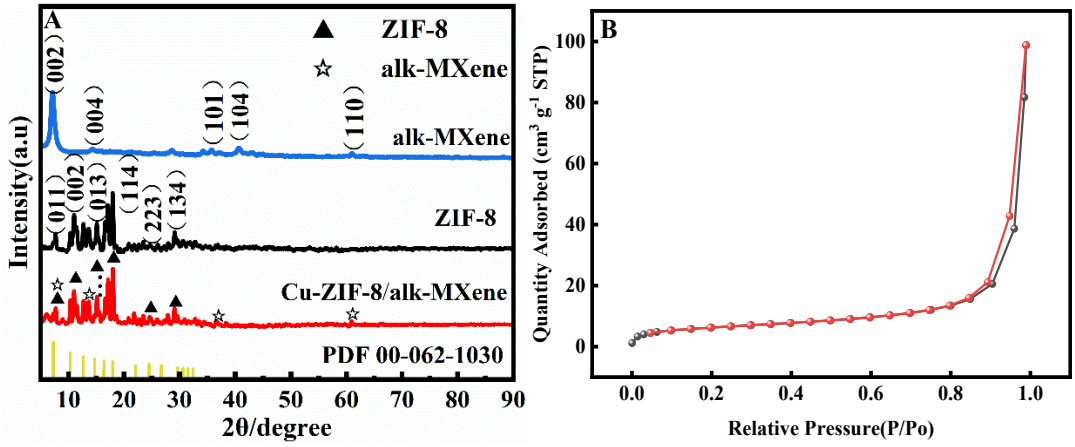
The XRD patterns of alk-MXene, ZIF-8, and the Cu-ZIF-8/alk-MXene composite are shown in Fig. 2A. The XRD pattern of ZIF-8 exhibits sharp characteristic diffraction peaks at $2\theta \approx 7.3°$ (011), 10.4° (002), 12.7° (112), 14.7° (013), 16.4° (114), among others. These diffraction peak positions match those of standard ZIF-8 crystals,

indicating the successful preparation of crystalline ZIF-8 [34, 36]. For alk-MXene, its XRD pattern exhibits a strong and sharp (002) characteristic peak at $2\theta \approx 6.0°$, accompanied by characteristic diffraction peaks of the MXene layered structure, such as (004) (~12.0°), (101) (~34.0°), (104) (~37.0°), (110) (~60.0°), which are characteristic of the MXene layered structure, confirming its typical layered crystal structure [21, 37]. The diffraction profile of the Cu-ZIF-8/alk-MXene composite displays the characteristic reflections of both alk-MXene and ZIF-8, with the intensity of the ZIF-8 peaks significantly enhanced and their shapes becoming sharper [38]. The above results confirm that Cu-ZIF-8/alk-MXene composite have been successfully synthesized.

Fig. 2(B-C) shows the N_2 adsorption-desorption isotherm and pore-size distribution of Cu-ZIF-8/alk-MXene. The isotherm is Type IV with an H3-type hysteresis loop, consistent with slit-like mesopores generated by stacked layered particles [32, 39, 40]. The measured BET specific surface area is 22.644 $m^2 \cdot g^{-1}$, the reported average pore diameter is 26.99 nm, and the N_2-accessible pore volume is 0.1528 $cm^3 \cdot g^{-1}$ (Table S2). These mesoporous dimensions are substantially larger than the intrinsic ZIF-8 aperture and are therefore consistent with hierarchical interparticle/interlayer voids that can accommodate and transport TC. Accordingly, the N_2 sorption data support a mechanism in which TC reaches accessible external/defect metal sites through the composite-scale mesoporous network rather than diffusing through the intrinsic ZIF-8 micropore windows.

Fig. 2D presents the FTIR spectrum of the Cu-ZIF-8/alk-MXene composite. There

were significant changes before and after the adsorption of TC. Among them, the -OH group shifted from 3385cm^{-1} to 3402 cm^{-1}, and the peak intensity significantly increased. This phenomenon indicates that hydrogen bonding interactions have formed between the -OH groups in the composite and the TC molecules [41, 42]. The band at 2923 cm^{-1} is assigned to the -CH_2 stretching absorption. The red-shift of characteristic peaks spanning 1571 cm^{-1} to 1566 cm^{-1} is ascribed to the C=C stretching vibration. The peak position variation in the range of 1429 cm^{-1} to 1422 cm^{-1} correlates with the stretching vibrations of -CH_3/-COOH. The observed red-shifts at 752-755 cm^{-1} and 418-421 cm^{-1} confirm the presence of M-O (M: Zn, Cu, Ti) bonds. The aforementioned peak shifts can be rationalized by a metal-bridged proton exchange process between TC and the surface -COOH moieties of the composite. In this process, the H^+ protons from the carboxylic groups undergo ligand exchange with TC molecules, leading to the formation of COO-M-TC ternary complexes. Such spectral transformation is indicative of new chemical bond generation, which strongly implies the co-occurrence of multiple adsorption mechanisms and synergistic interactions across distinct active sites.



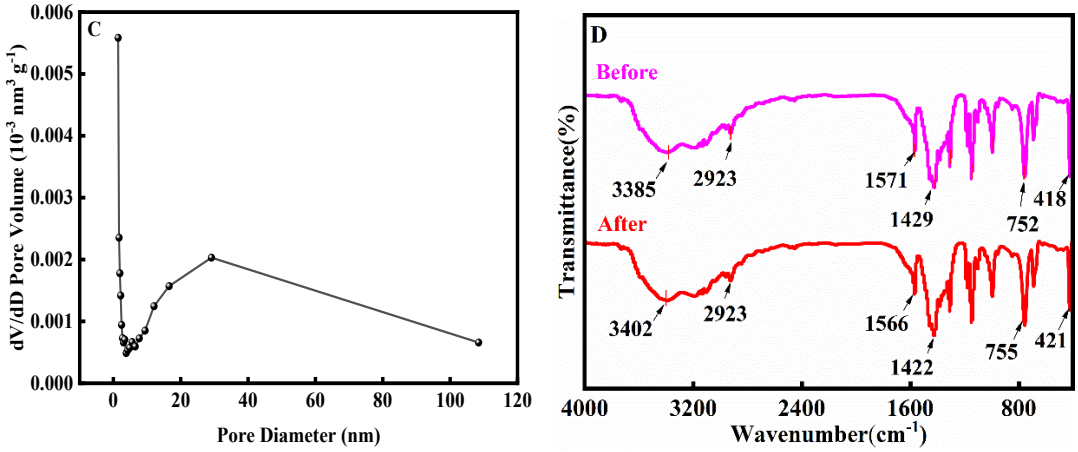


Fig. 2. Structural and textual characterization of the as-prepared samples. (A) XRD patterns of alk-MXene, ZIF-8, and Cu-ZIF-8/alk-MXene; (B) adsorption-desorption isotherms of Cu-ZIF-8/alk-MXene; (C) particle size distribution of Cu-ZIF-8/alk-MXene; (D) FTIR spectra of Cu-ZIF-8/alk-MXene before and after adsorption.

Fig. 3(A-F) presents high-resolution C 1s 、N 1s、O 1s、Cu 2p、Zn 2p and Ti 2p spectrum. The high-resolution C 1s spectrum shows that the binding energy (284.8 eV) of C-C, as well as the peak shape and peak area, remain unchanged before and after adsorption, indicating that the carbon framework of the composite material remains stable during the adsorption process. The binding energy of C-N/C-O moves from 286.1eV to 285.9eV after adsorption of TC, with a significant shift (0.2eV) and a significant increase in the relative area of the peak, which can be attributed to the introduction of C-O and C-N structures that exist in large numbers in TC molecules [15, 21, 43]. The high-resolution N 1s spectrum contains two fitted components at 400.1 and 398.9 eV. After adsorption, the amino and amide groups contained in the TC molecules are adsorbed onto the surface of the material, resulting in an increase in the intensity of the C=N peak (398.9 eV), indicating that TC has been successfully loaded on the surface of the material. Fig. 3(C) shows the characteristic peaks at 533.1 eV and 531.4

eV after the peak-to-peak fitting of the O1s spectrum. After adsorbing TC, the C-O/C=O (533.1 eV) peak shifted to a lower binding energy to 532.6 eV (a shift of approximately 0.5 eV), and at the same time, the M-O peak at 531.4 eV also showed a slight shift. It is speculated that the phenolic hydroxyl groups and other oxygen-containing functional groups in the TC molecule interacted with the oxygen-containing functional groups or metal sites on the material surface through hydrogen bonds, resulting in an increase in the electron cloud density on the oxygen atoms and a decrease in the binding energy.

Fig. 3(D-F) display the high-resolution XPS spectra of Zn 2p, Cu 2p and Ti 2p. After TC adsorption, the Cu 2p high-resolution spectrum shows that the Cu $2p_{1/2}$ peak shifts to a lower binding energy by 0.7 eV to 933.9 eV, while the Cu $2p_{3/2}$ peak slightly shifts to 932.6 eV. This phenomenon indicates an increased electron cloud density of Cu atoms, which can be ascribed to the electron transfer from the electron-rich groups (e.g., $-NH_2$, -OH, C=O) of TC (acting as an electron donor) to Cu atoms after adsorption, forming strong coordination interactions with Cu sites [43]. This result confirms that Cu sites are the dominant active centers for TC adsorption. The Zn 2p high-resolution spectrum shows that the binding energies of the two fitted peaks before and after adsorption changed very little (from 1021.6 eV to 1021.7 eV; from 1044.8 eV to 1044.7 eV), which proves that there was no significant electron transfer or strong coordination effect of Zn before and after adsorption of TC. It might also be due to the highly stable coordination environment of Zn before and after adsorption [17, 43]. The Ti 2p high-resolution spectrum shows five fitting peaks, corresponding to different chemical states of Ti (III) and Ti (IV). After adsorption, no significant redox reactions or strong

chemical coordination interactions occurred at the Ti sites. The adsorption of TC at the Ti site may be due to electrostatic interactions [23, 28, 44]. In summary, TC mainly forms strong coordination bonds with the Cu sites on the surface of Cu-ZIF-8/alk-MXene materials through its electron-rich groups (-NH_2, -OH, C=O), thereby forming stable surface complexes as evidenced by the significant shift of Cu 2p towards lower binding energies. Hydrogen bonds are formed between -OH in TC and the C-O functional groups on the material surface (the C-O peak in O 1s moves 0.5 eV towards a lower binding energy). Additionally, the C=C peak in C 1s demonstrates the existence of electrostatic attraction and π-π stacking interactions, as well as weak physical adsorption at Zn and Ti sites. Meanwhile, distinct characteristic peaks of Cu 2p, Zn 2p and Ti 2p are observed in the XPS survey scan spectrum, demonstrating the successful synthesis of the Cu-ZIF-8/alk-MXene material.

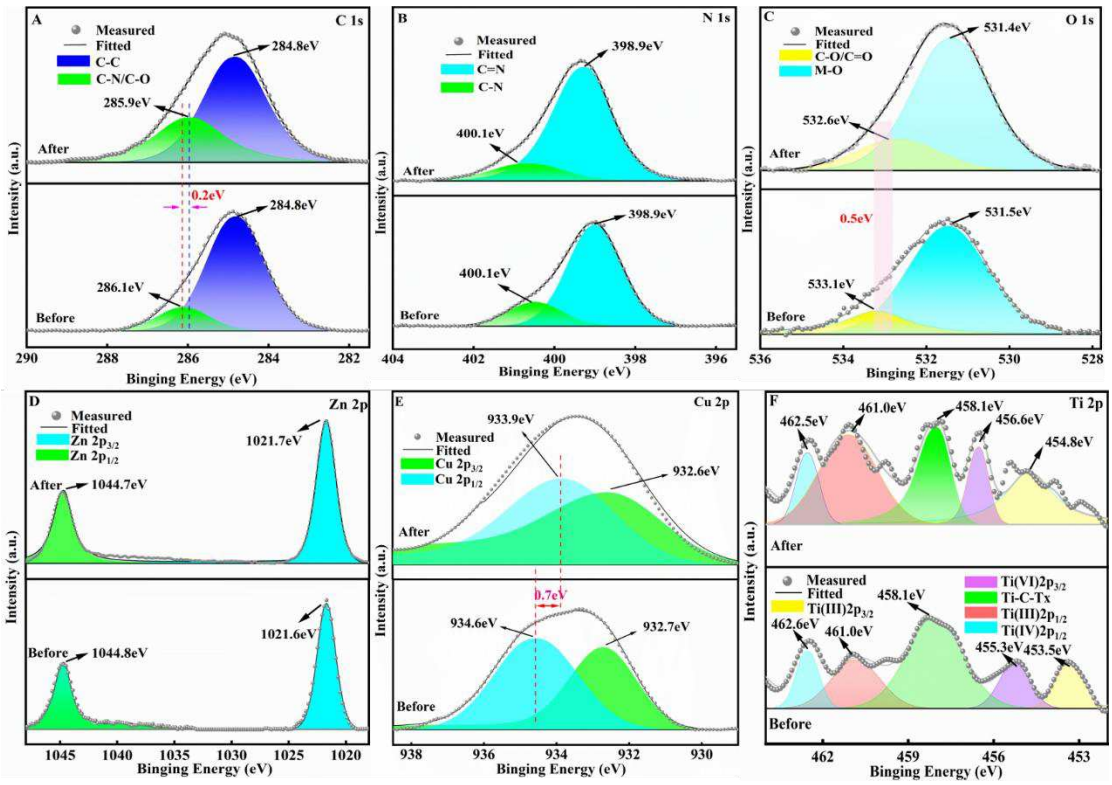


Fig. 3. High-resolution XPS spectra of the as-prepared Cu-ZIF-8/alk-MXene composite. (A) C 1s; (B) N 1s; (C) O 1s; (D) Zn 2p; (E) Cu 2p; and (F) Ti 2p.

3.2 Batch adsorption experiment

3.2.1 Adsorption kinetics

Fig. 4(A-D) presents the analysis of the adsorption process of TC by Cu-ZIF-8/alk-MXene material within the range of 0-840 minutes using the kinetic analysis method, with Pseudo-first-order, Pseudo-second-order, Elovich, and intra-particle diffusion models. The results show that the Pseudo-second-order kinetic model ($R^2 = 0.998$) has better fitting correlation than the Pseudo-first-order kinetic model ($R^2 = 0.991$), and the theoretical equilibrium adsorption amount is in good agreement with the experimental results (supporting information Table S3), indicating that the adsorption process is mainly controlled by chemical adsorption. The Elovich model also exhibits a high correlation with the experimental data ($R^2 = 0.998$), This further confirms that chemical adsorption is the main adsorption process [45, 46]. Additionally, the particle internal diffusion model reveals that van der Waals forces facilitate the internal mass transfer process of TC molecules. Combined with the three-segment linear fitting results of the intraparticle diffusion model, the three-segment curve of qt versus $t_{1/2}$ clearly characterizes the multistage mass transfer features of the adsorption process for detailed internal diffusion parameters, see supporting information Table S4: the initial stage ($t_{1/2} \approx 0$-13) is dominated by outward diffusion, with the mesoporous topology and abundant surface active sites unique to MXene materials driving the rapid mass transfer of TC molecules; the transition stage ($t_{1/2} \approx$ 12-28) is limited by intraparticle diffusion, with

the adsorbate migrating through the material's pore structure toward deeper active sites; and the final stage ($t_{1/2} \approx 28$ and beyond) sees adsorption gradually approaching equilibrium, at which point mass transfer resistance significantly increases and active site saturation leads to a slowdown in the rate of increase in adsorption uptake. In particular, the fitting curve does not pass through the origin, indicating that TC's internal diffusion is not the only process, and TC's mass transfer process may be affected by the boundary layer effect [47, 48]. In conclusion, the adsorption of TC by Cu-ZIF-8/alk-MXene conforms to the Pseudo-second-order kinetic model, and it is confirmed that electrostatic attraction is the main adsorption mechanism, as well as the existence of van der Waals forces and diffusion adsorption mechanisms.

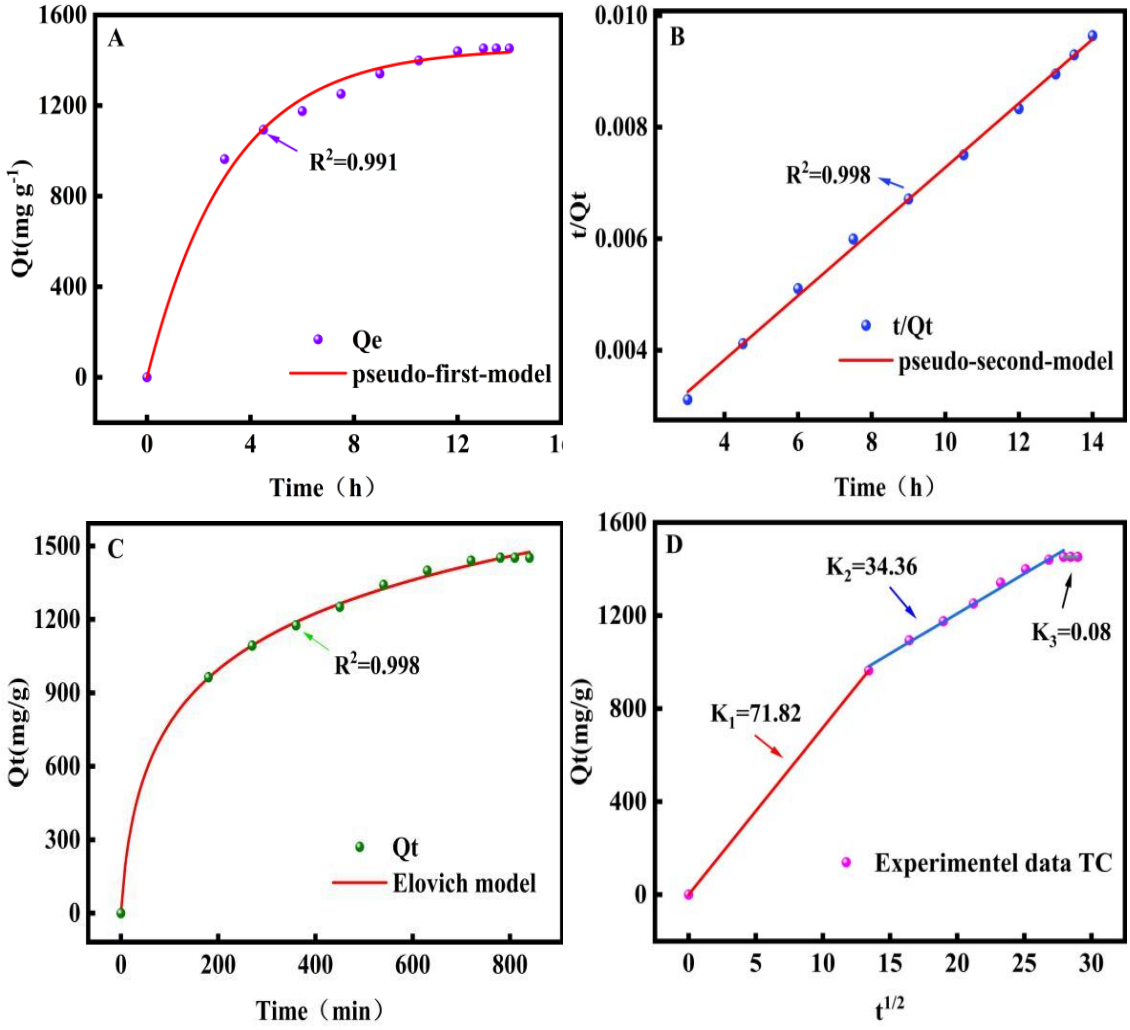


Fig. 4. Kinetic fitting curves for TC adsorption onto Cu-ZIF-8/alk-MXene. (A) Pseudo-first-order model; (B) Pseudo-second-order model; (C) Elovich model, (D) intraparticle diffusion model.

3.2.2 Adsorption isotherm

Fig. 5A shows the adsorption capacity of this composite material for tetracycline at different initial concentrations. With the increase of the initial TC concentration, the adsorption capacity of Cu-ZIF-8/alk-MXene gradually increases. Under the condition of high TC concentration, due to the occupation of the metal active center, the adsorption capacity tends to stabilize [33]. A systematic analysis of the adsorption

behavior of TC by the Cu-ZIF-8/alk-MXene composite was conducted using the Langmuir, Freundlich, and Sips adsorption isotherm models as shown in Fig. 5(B-C). The analysis results indicate that the coefficient of determination for the Langmuir model (R^2 = 0.9965) is significantly higher than that for the Freundlich model (R^2 = 0.9780), while the Sips model also exhibits a high correlation (R^2 = 0.9971), It is proved that TC is adsorbed on the surface of Cu-ZIF-8/alk-MXene as a monolayer. At low concentrations, the abundant adsorption sites on the material surface enable TC to be rapidly adsorbed by the material, but at high concentrations, due to the occupation of many adsorption sites, the adsorption capacity tends to stabilize [48, 49]. The fitting results of the three isothermal adsorption curves are listed in Table 1. The maximum TC adsorption capacity estimated using the Langmuir model (q_{max} =1631.1 $mg \cdot g^{-1}$) The maximum TC adsorption capacity estimated using the Langmuir model (q_{max} = 1631.1 $mg \cdot g^{-1}$) is consistent with the experimental values and the results of molecular dynamics fitting [27, 50-53]. Moreover, the adsorption capacity of Cu-ZIF-8/alk-MXene is higher than that of other adsorbents reported in the literature. Table 2 presents a comparison of the adsorption performance of Cu-ZIF-8/alk-MXene with that of the reported adsorption materials.

In conclusion, the adsorption mechanism of the Cu-ZIF-8/alk-MXene material is mainly dominated by Langmuir monolayer homogeneous adsorption, and the adsorption sites are evenly distributed. There is no obvious interaction between the adsorbed molecules and non-homogeneous surface features are present. The Sips fitting curve with ns $\approx$ 1 further confirms that the material's adsorption is approaching

homogeneity and is mainly monolayer adsorption. The n > 1 in the Freundlich model confirms that this adsorption is a spontaneous and easily occurring adsorption process. In summary, the above results confirm that Cu-ZIF-8/alk-MXene exhibits monolayer homogeneous adsorption behavior.

Table 1 Langmuir, Freundlich and Sips adsorption isotherm parameters

Classification	Parameters	Values
Langmuir	R^2	0.9965
	q_{max} (mg g^{-1})	1631.1
	kl (L mg^{-1})	0.04418
Freundlich	R^2	0.9780
	kf (mg g^{-1})(L mg^{-1})$^{1/n}$	195.08
	n	2.34
Sips	q_{max} (mg g^{-1})	1744.33
	ks (L mg^{-1})	0.03718
	ns	1.09929

Table 2 Adsorption uptake of Various Adsorbents for TC

Adsorbent	Absorption capacity（$mg \cdot g^{-1}$）	TC concentration ($mg \cdot L^{-1}$)	pH	Temperature (K)	Adsorption Model	Ref
Cu-ZIF-8/alk-MXene	1631.1	10-200 $mg \cdot L^{-1}$	7.0	298	Langmuir	This work
alk-MXene/ZIF	1053.30	50-300 $mg \cdot L^{-1}$	7.0	298	Langmuir	[28]
ZIF-8-LS	48.00	10-50 $mg \cdot L^{-1}$	6.8	298	Langmuir	[54]
Cu-ZIF-8	892.40	10-70 $mg \cdot L^{-1}$	6.0	298	Langmuir	[21]
Cu-Co MOF	768.50	10-450 $mg \cdot L^{-1}$	7.0	298	Langmuir	[29]
Fe_3O_4@ZIF-8@ZIF-67	659.80	20-160 $mg \cdot L^{-1}$	7.0	298	Langmuir	[4]

3.2.3 Thermodynamics of Adsorption

Fig. 5C shows the plot of lnKc versus 1/T for the Cu-ZIF-8/alk-MXene composite. The thermodynamic parameters obtained from the experimental fitting are provided in the supporting information Table S5. The R^2 value for the Van't Hoff equation fit is 0.995, indicating a good linear relationship between lnKc and 1/T and confirming the reliability of the calculated thermodynamic parameters. As shown in supporting information Table S5, ΔH = 15.85 kJ mol^{-1} is a positive value, demonstrating the endothermic nature of the adsorption process. When the temperature increases from 298 K to 338 K, qe increases from 1244.13 $mg \cdot g^{-1}$ to 1392.84 $mg \cdot g^{-1}$, consistent with $\Delta H > 0$. At high temperatures, the increased kinetic energy of TC molecules makes it easier to reach the energy threshold required for binding to adsorption sites. Furthermore, the coordination activity of surface-active sites, such as the Cu-ZIF-8

metal sites, is enhanced after "thermal activation," facilitating the binding of TC to adsorption sites. The positive ΔS value reflects an increase in interfacial disorder during adsorption, which may result from disruption of the ordered arrangement of TC molecules on the adsorbent surface and the displacement of interlayer water by adsorbed TC, leading to increased disorder in the microscopic state of the interface. ΔG is negative at all temperatures (ΔG = -9.60 kJ mol^{-1} at 298 K and ΔG = -13.01 kJ mol^{-1} at 338 K), and its absolute value increases with rising temperature, indicating that adsorption proceeds spontaneously and that the higher the temperature, the stronger the spontaneity. In summary, the adsorption of TC onto Cu-ZIF-8/alk-MXene composites follows endothermic, spontaneous, and entropy-increasing thermodynamic behaviors within the investigated temperature range. The spontaneity and entropy increase indicate that the adsorption does not require external energy input and that the microscopic state of the system becomes more disordered, further supporting the mechanism of strong interactions between TC and multi-site sites, with mass transfer and binding occurring synergistically [14, 55].

3.2.4 The Effect of pH

To investigate the adsorption behavior of TC by Cu-ZIF-8/alk-MXene composites, the initial pH of the solution is a key influencing factor, as it is closely related to the form of TC and the charge state at the surface of the adsorbent at different pH values [45, 46]. As illustrated in Fig. 5D, the adsorption capacity of the material was only 576 $mg \cdot g^{-1}$ at pH = 2. It increased significantly within the pH range of 4-10, reaching a maximum of 1377.25 $mg \cdot g^{-1}$ at pH=6, before declining sharply at pH=12. This trend

can be attributed to electrostatic interactions involving protonation and the adsorption of TC. Prior research has indicated that the speciation of TC varies with pH: when pH < 3.32, TC exists predominantly exists as the cationic species TC^{+}; when 3.32 < pH < 7.78, it exists as the electrically neutral TC^{0} form; when 7.78 < pH < 9.58, it exists as the negatively charged TC^{-} form; and when pH > 9.58, it exists as the TC^{2-} form [28, 56]. Under the strongly acidic condition of pH = 2, the oxygen-containing groups on the surface of the Cu-ZIF-8/alk-MXene material and the N-containing groups of the imidazole ligands in Cu-ZIF-8 are highly prone to undergo protonation and form strong electrostatic repulsion with the positively charged TC^{+}. Moreover, the dissolution of metal sites in the Cu-ZIF-8 framework under strong acid conditions also leads to a significant reduction in the coordination adsorption sites, thereby reducing the adsorption capacity of the material [57]. Within the pH range of 4-10, as the pH value increases, the metal sites in the material act as Lewis acid sites and form strong coordination interactions with the electron-rich groups on TC molecules. Meanwhile, the nitrogen-containing groups in the material form hydrogen bonds with the hydroxyl and amino groups on TC molecules, and intense π-π stacking interactions also occur between the imidazole rings of ZIF-8 and the benzene rings of TC. The synergistic effect of multiple mechanisms enables the material to reach its maximum adsorption capacity [52, 57]. At highly alkaline conditions (pH approaching 14), the surface hydroxy groups (-OH) on the material are nearly fully deprotonated, transforming into negatively charged surface oxo sites ($\equiv$-O^{-}). Concurrently, Cu-ZIF-8 also carries negative charges. At this point, a large number of negative charges on the material

surface generate extremely strong electrostatic repulsion with the negatively charged TC^{2-}. In addition, the metal active sites bind with OH^- in the solution to form insoluble metal oxide precipitates. This process completely deprives the metal ions of their coordination ability toward TC, resulting in the total loss of coordination adsorption sites in the material, and thus the adsorption capacity is drastically reduced once again [57]. Combining the above experimental observations with the XPS spectra of C 1s, O 1s, Cu 2p, Zn 2p and Ti 2p, the maximum adsorption capacity of Cu-ZIF-8/alk-MXene can be attributed to the synergistic effects of metal coordination, electrostatic interaction and π-π stacking.

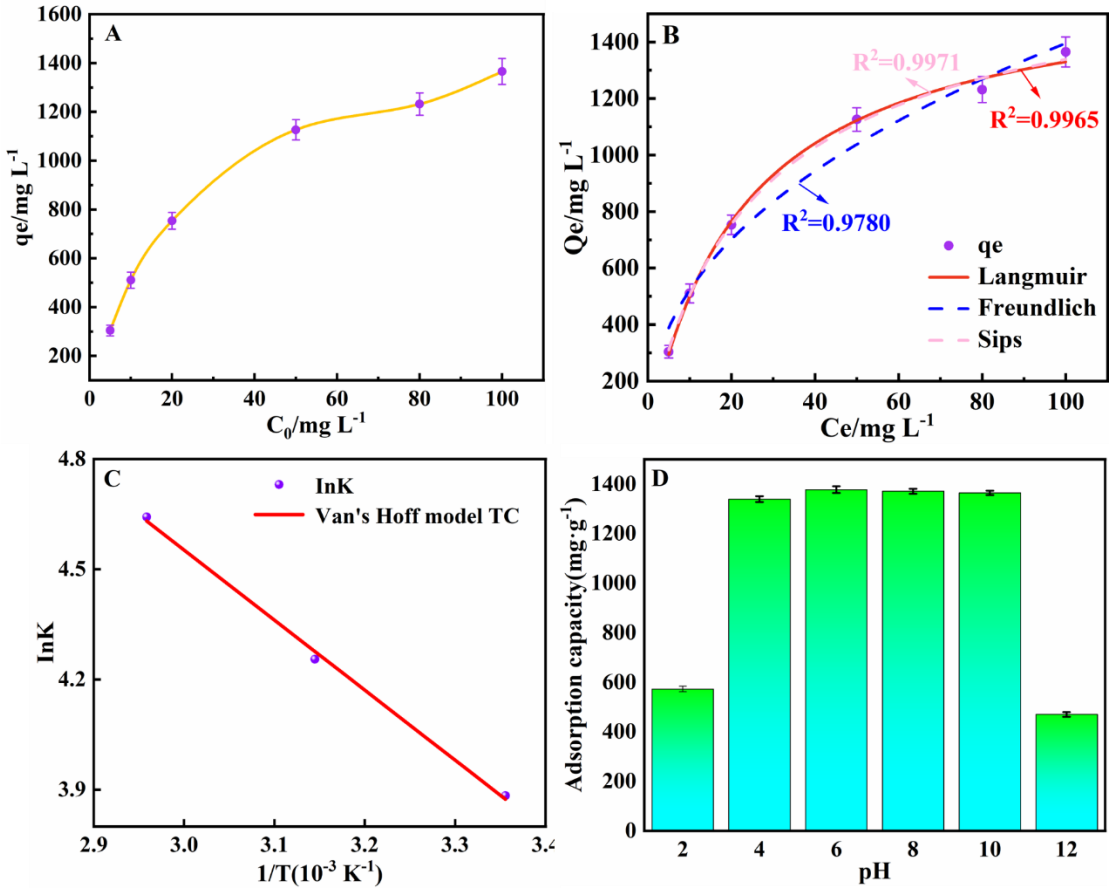


Fig.5. (A) Impact of TC concentration on adsorption; (B) Isotherm model for TC adsorption by Cu-ZIF-8/alk-MXene; (C)Van't Hoff plot for the Cu-ZIF-8/alk-MXene

adsorption process; (D) Effect of different pH values on the adsorption temperature (TC) of Cu-ZIF-8/alk-MXene.

3.2.5 The Effect of coexisting ions

To evaluate the applicability of Cu-ZIF-8/alk-MXene in complex aqueous environments, the effects of different coexisting cations (Na^+, K^+, $Ca^{2+}$and Mg^{2+}) at concentrations of 50, 100, and 150 $mg \cdot L^{-1}$ were investigated, as shown in Fig. 6A, the adsorption uptake for TC in tap water decreased significantly compared to that in deionized water. The presence of metal cations has varying degrees of influence on the material's adsorption of total chromium (TC) in water. Notably, the presence of divalent cations (Ca^{2+} and Mg^{2+}) has a more significant impact on adsorption uptake compared with the effects of the monovalent ions Na^+ and K^+. This phenomenon can be attributed to the low charge density of monovalent metal ions, which results in weak electrostatic interactions with negatively charged sites on the material surface, making it difficult for them to compete effectively with TC molecules through strong electrostatic repulsion. In contrast, divalent ions have a high charge density and can significantly weaken the electrostatic attraction between the adsorbent and TC. Moreover, Cu^{2+} in the material serves as the key active site for TC adsorption. Mg^{2+} and Ca^{2+} form stable metal-TC complexes with TC molecules, competing with Cu^{2+} for coordination sites on TC, thereby reducing the effective coordination sites of Cu^{2+} and significantly decreasing the adsorption capacity [58]. Compared to Ca^{2+}, Mg^{2+} has a smaller ionic radius, stronger ability to neutralize surface charges on materials, and it is more likely to compete with TC for complexation, resulting in a more pronounced inhibitory effect

than Ca^{2+} [59]. The adsorption effect of cations on TC follows the order: $Mg^{2+} > Ca^{2+} > Na^{+} > K^{+}$.

3.3 Reusability

To assess the adsorption-desorption cycling stability of the Cu-ZIF-8/alk-MXene composite toward TC, regeneration experiments were conducted using anhydrous ethanol. As shown in the data in Fig. 6B, the TC adsorption uptake exhibited a gradual decline with increasing cycle numbers, but remained at a relatively high level overall: even after five cycles, the adsorption uptake still reached 1283.51 $mg \cdot g^{-1}$.This performance decline may be attributed to factors such as structural damage to the adsorbent and a reduction in active sites during the regeneration process. However, judging from the overall trend, Cu-ZIF-8/alk-MXene still exhibits good cycling stability and can be repeatedly applied in the adsorption and removal of TC, demonstrating significant potential for practical applications [60].

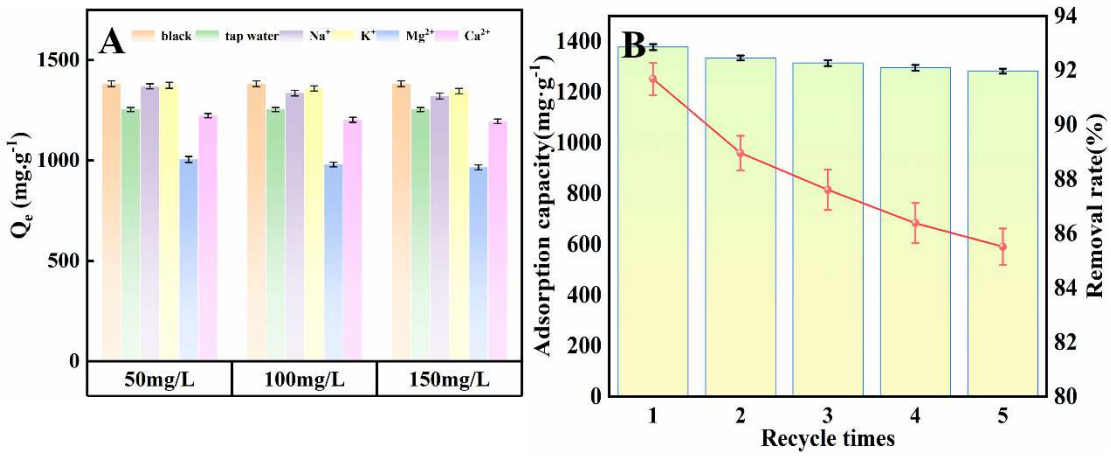


Fig. 6. (A) Effects of different concentrations of coexisting cations and water matrices on TC adsorption by Cu-ZIF-8/alk-MXene; (B) Reusability of Cu-ZIF-8/alk-MXene during five adsorption–desorption cycles.

3.4 DFT

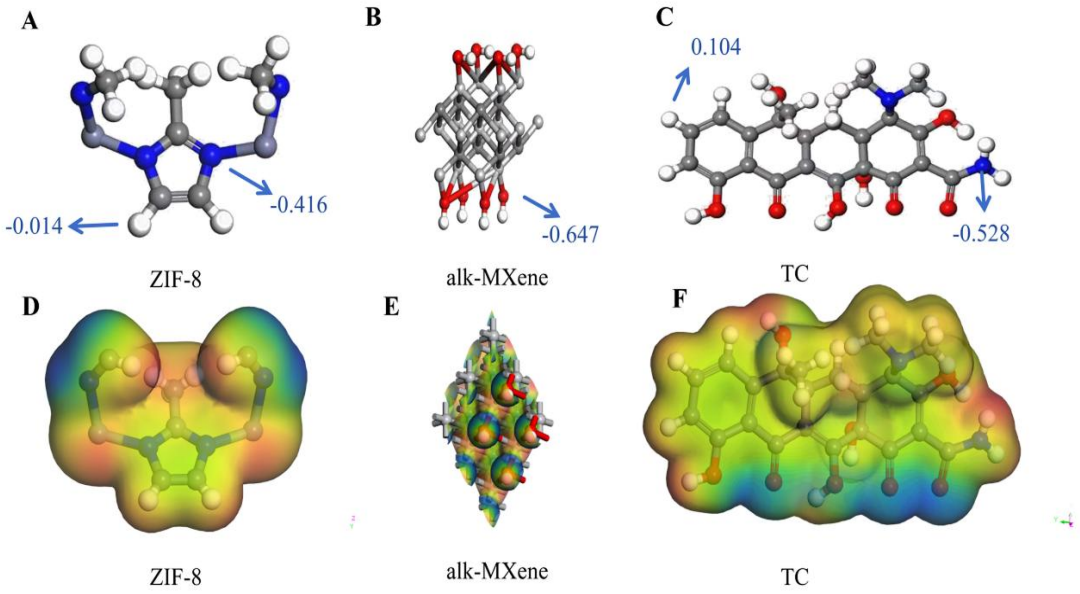
To further elucidate the molecular-level interaction mechanisms between TC and Cu-ZIF-8/alk-MXene, we performed DFT calculations by analyzing the electrostatic surface charge and molecular electrostatic potential distributions before and after adsorption [23, 28]. Fig. 7(A,D) for the ZIF-8 domain, the charge on the nitrogen atom coordinating with Zn^{2+} changed from -0.416 to -0.328, indicating that TC adsorption caused a charge redistribution around the Zn-N coordination environment. It indicates that ZIF-8 has the ability to accept protons or to combine with cations/electron-deficient groups [60]. Fig. 7(B,E) shows that the surface of alk-MXene has a very strong negative potential region (-0.647 eV), mainly due to the -O, -OH, -F groups on the surface and the electron-rich areas in the layered structure, making it highly nucleophilic and easily undergoing electrostatic attraction with the electron-deficient areas. Fig. 7(C,F) demonstrates that the TC molecule has a amphiphilic potential distribution. The negative potential (-0.528 eV) is concentrated near oxygen-rich groups such as ketone groups and phenolic hydroxyl groups, while the positive potential (0.104 eV) is concentrated near amine groups and specific hydrogen atoms. This provides a basis for TC to adsorb on the material surface through electrostatic interactions [61, 62].

Fig.7 (G,I) shows that the Cu-ZIF-8/alk-MXene composite changes the charge distribution at the metal site and ligand interface after Cu is introduced into ZIF-8 (a strong negative potential region of -0.733 eV coexists with a positive potential region of 0.109 eV). The strong negatively charged groups (-O, -OH) on the alk-MXene surface exhibit strong electrostatic attraction to the positively charged Cu sites or

imidazole ligands in Cu-ZIF-8. Moreover, the unsaturated coordination sites of Cu readily coordinate with the -O or -OH groups on the alk-MXene surface, forming a stable heterojunction structure. The presence of this interaction mechanism is also confirmed by Cu 2p XPS analysis [63-65]. Fig. 7(H,J) further confirms that the adsorption of TC onto the Cu-ZIF-8/alk-MXene composite results from a synergistic effect of multiple mechanisms, in which negatively charged oxygen-rich groups in TC molecules (-0.556 eV, -0.671 eV) are strongly electrostatically attracted to positively charged regions on the composite, while positively charged amine groups in TC (0.128 eV, 0.210 eV) interact strongly with the highly negative potential areas on the alk-MXene surface (-0.328 eV) [28]. In Cu-ZIF-8, the metal sites of Cu accept the lone pair electrons of the electron-rich oxygen or nitrogen atoms in the TC molecule, forming Cu-O or Cu-N coordination bonds, which significantly enhances the adsorption affinity, and is consistent with the O 1s results in XPS [24, 66]. The hydroxyl and amino groups (hydrogen donors) on the TC molecule form hydrogen bonds with the oxygen/fluorine hydrogen acceptors on the surface of alk-MXene or the nitrogen atoms on the imidazole ring in ZIF-8 [32, 62]. The π-π stacking interactions formed between multiple aromatic rings in the TC molecule and the imidazole rings of ZIF-8 as well as the layered structure of MXene [43], further enhance adsorption stability, a conclusion consistent with the XPS C 1s characterization results. The porous structure of ZIF-8 allows TC molecules to enter its pores, resulting in a spatial confinement effect [66].

In summary, the results of DFT calculation combined with FTIR and XPS analysis revealed a multi-mechanism synergistic adsorption process of TC by Cu-ZIF-8/alk-

MXene. Among them, electrostatic interaction, coordination with Cu sites, interfacial hydrogen bonds, and π-π stacking jointly constitute an efficient adsorption system. The combination of Cu-ZIF-8 and alk-MXene in the composite material effectively regulates the charge distribution at the material interface, providing more adsorption active sites for TC adsorption, significantly enhancing the adsorption performance of TC, its adsorption mechanism such as Fig. 8.



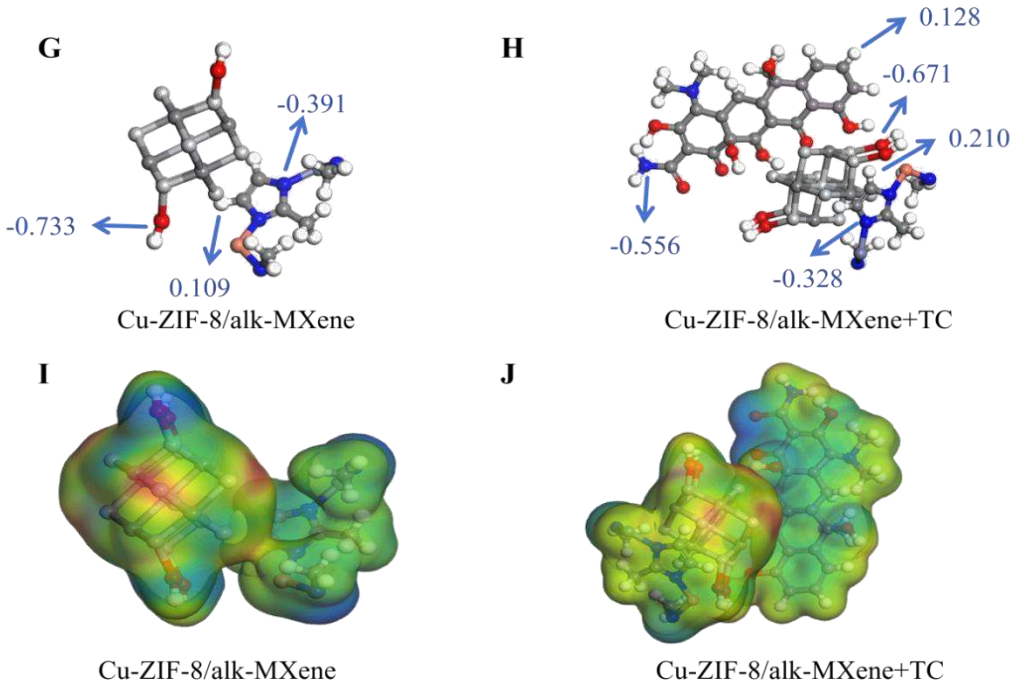


Fig. 7. (A) Electrostatic surface charge of ZIF-8; (B) Electrostatic surface charge of alk-MXene; (C) Electrostatic surface charge of TC; (D) Two-dimensional electrostatic potential map of the ZIF-8 molecule; (E) Electrostatic potential map of alk-MXene; (F) Two-dimensional electrostatic potential map of the TC molecule. (G) Electrostatic surface charge of Cu-ZIF-8/alk-MXene; (H) Electrostatic surface charge of Cu-ZIF-8/alk-MXene + TC; (I) Electrostatic potential map of Cu-ZIF-8/alk-MXene; (J) Electrostatic potential map of Cu-ZIF-8/alk-MXene + TC.

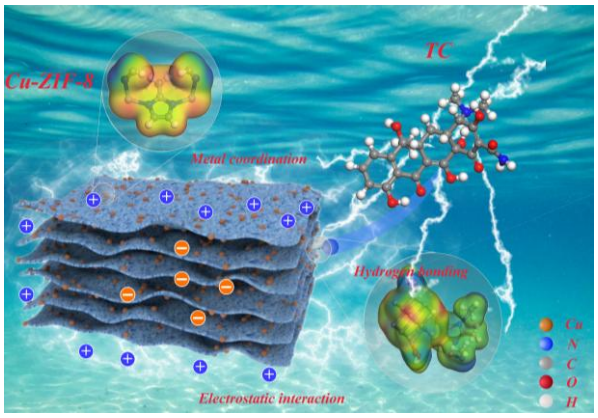


Fig. 8. Mechanism of TC adsorption by Cu-ZIF-8/alk-MXene.

4. Conclusion

In this study, a novel Cu-ZIF-8/alk-MXene composite material was successfully synthesized through in-situ growth and post-modification strategies. This approach achieved the integration of Cu doping and the embedding of 2D ZIF-8 nanosheets to enhance the metal adsorption sites, as well as the increase in the types of functional groups and layer spacing of alk-MXene in the material. The composite exhibits outstanding adsorption performance toward TC, with a maximum adsorption capacity of 1631.1 $mg \cdot g^{-1}$, far exceeding that of previously reported materials. It maintains high adsorption efficiency across a broad pH range (4.0-10.0). Kinetic and thermodynamic analyses indicate that the adsorption process follows a Pseudo-second-order kinetic model and the Langmuir monolayer adsorption model, revealing that chemical adsorption is the dominant mechanism. The adsorption mechanism reveal that the material achieves efficient TC capture through multiple interactions, including electrostatic attraction, metal coordination, and hydrogen bonding, with the introduction of Cu^{2+} significantly enhancing the coordination interactions. Furthermore, the material exhibits good adsorption selectivity even under the interference of coexisting ions. After five cycles, the TC adsorption capacity remains at 1283.51 $mg \cdot g^{-1}$, demonstrating excellent practical application potential and cycle stability. This study not only provides new insights into the design of MXene-based composite adsorbents but also offers an innovative material solution for the efficient removal of antibiotic pollutants from water through synergistic multi-mechanism effects.

CRediT authorship contribution statement

Handong Leng: Methodology, Investigation, Formal analysis, Writing-original draft. **Xingyu Yang：** Methodology, Investigation, Formal analysis. **Xu Liu:** Methodology, Writing-review & editing, Supervision, Funding acquisition. **Yingying Zuo:** Writing-review & editing. **Yuhua Gao:** Investigation. **Hanwen Cui:** Investigation, Data curation. **Ziyan Wang:** Investigation, Data curation. **Penghui Wu:** Investigation. **Boxing An:** Investigation. **Zhengqi Liang:** Investigation. **Hai Liang:** Investigation. **Kangjun Wang:** Supervision. **Yushan Li:** Resources, Supervision, Writing-review & editing, Funding acquisition.

Declaration of competing interest

The authors declare that they have no known competing financial interests or personal relationships that could have appeared to influence the work reported in this paper.

Data availability

Data will be made available on request.

Acknowledgements

This work was financially supported by the Foundation of Liaoning Key Laboratory of Chemical Additive Synthesis and Separation (ZJKF2504, ZJKF2403), Fundamental Scientific Research Fund System Pilot project of Hebei Academy of Sciences （2026PF13）.

Supplementary materials

Supplementary material associated with this article can be found, in the online version.

References

[1] C. Liang, Y. Tang, X. Zhang, H. Chai, Y. Huang, P. Feng, ZIF-mediated N-doped hollow porous carbon as a high performance adsorbent for tetracycline removal from water with wide pH range, Environmental Research 182 (2020) 109059. https://doi.org/10.1016/j.envres.2019.109059.

[2] Y. Zhou, F. Fang, Q. Lv, Y. Zhang, X. Li, J. Li, Simultaneous removal of tetracycline and norfloxacin from water by iron-trimesic metal-organic frameworks, Journal of Environmental Chemical Engineering 10(3) (2022) 107403. https://doi.org/10.1016/j.jece.2022.107403.

[3] B. Jeyhoon, V. Safarifard, Harnessing light: advanced photodegradation of tetracycline using NH2-MIL-101(Cr)@ZIF-67 in water, Journal of Nanoparticle Research 26(11) (2024). https://doi.org/10.1007/s11051-024-06156-3.

[4] X. Song, J. Mo, Y. Fang, S. Luo, J. Xu, X. Wang, Synthesis of magnetic nanocomposite Fe3O4@ZIF-8@ZIF-67 and removal of tetracycline in water, Environmental Science and Pollution Research 29(23) (2022) 35204-35216. https://doi.org/10.1007/s11356-021-18042-9.

[5] Y. Feng, H. Wang, J. Xu, X. Du, X. Cheng, Z. Du, H. Wang, Fabrication of MXene/PEI functionalized sodium alginate aerogel and its excellent adsorption behavior for Cr(VI) and Congo Red from aqueous solution, Journal of Hazardous Materials 416 (2021) 125777. https://doi.org/10.1016/j.jhazmat.2021.125777.

[6] S. Pal, K. Madane, A.A. Kulkarni, Antisolvent based precipitation: Batch, capillary flow reactor and impinging jet reactor, Chemical Engineering Journal 369 (2019) 1161-1171. https://doi.org/10.1016/j.cej.2019.03.107.

[7] R. Zheng, Y. Chen, J. Wang, J. Song, X.-M. Li, T. He, Preparation of omniphobic PVDF membrane with hierarchical structure for treating saline oily wastewater using direct contact membrane distillation, Journal of Membrane Science 555 (2018) 197-205. https://doi.org/10.1016/j.memsci.2018.03.041.

[8] D. Hernández, B. Riaño, M. Coca, M. Solana, A. Bertucco, M.C. García-González, Microalgae cultivation in high rate algal ponds using slaughterhouse wastewater for biofuel applications, Chemical Engineering Journal 285 (2016) 449-458. https://doi.org/10.1016/j.cej.2015.09.072.

[9] M. Shahmansoori, S. Yaghmaei, N.M. Mahmoodi, Green synthesis of chitosan-ZIF67 composite beads for efficient removal of Malachite Green and Tetracycline, Chemical Engineering Science 304 (2025) 121017. https://doi.org/10.1016/j.ces.2024.121017.

[10] X. Han, Y. Huang, L. Ding, Y. Song, T. Li, P. Liu, Ti3C2Tx MXene Nanosheet/Metal–Organic Framework Composites for Microwave Absorption, ACS Applied Nano Materials 4(1) (2020) 691-701. https://doi.org/10.1021/acsanm.0c02983.

[11] I. Ihsanullah, MXenes (two-dimensional metal carbides) as emerging nanomaterials for water purification: Progress, challenges and prospects, Chemical Engineering Journal 388 (2020) 124340. https://doi.org/10.1016/j.cej.2020.124340.

[12] K. Ramadass, C.I. Sathish, G. Singh, S.M. Ruban, A.M. Ruban, R. Bahadur, G. Kothandam, T. Belperio, J. Marsh, A. Karakoti, J. Yi, A. Vinu, Morphologically tunable nanoarchitectonics of mixed kaolin-halloysite derived nitrogen-doped activated nanoporous carbons for supercapacitor and CO2 capture applications, Carbon 192 (2022) 133-144. https://doi.org/10.1016/j.carbon.2022.02.047.
[13] Y. Yao, X. Han, X. Yang, J. Zhao, C. Chai, Detection of Hydrazine at MXene/ZIF-8 Nanocomposite Modified Electrode†, Chinese Journal of Chemistry 39(2) (2021) 330-336. https://doi.org/10.1002/cjoc.202000398.
[14] C. Hao, G. Li, G. Wang, W. Chen, S. Wang, Preparation of acrylic acid modified alkalized MXene adsorbent and study on its dye adsorption performance, Colloids and Surfaces A: Physicochemical and Engineering Aspects 632 (2022) 127730. https://doi.org/10.1016/j.colsurfa.2021.127730.
[15] R. Wang, H. Cao, C. Yao, C. Peng, J. Qiu, K. Dou, N. Tsidaeva, W. Wang, Construction of alkalized MXene-supported CoFe2O4/CS composites with super-strong adsorption capacity to remove toxic dyes from aqueous solution, Applied Surface Science 624 (2023) 157091. https://doi.org/10.1016/j.apsusc.2023.157091.
[16] D. Sheng, X. Ying, R. Li, S. Cheng, C. Zhang, W. Dong, X. Pan, Polydopamine-mediated modification of ZIF-8 onto magnetic nanoparticles for enhanced tetracycline adsorption from wastewater, Chemosphere 308 (2022) 136249. https://doi.org/10.1016/j.chemosphere.2022.136249.
[17] T.V. Tran, A.A. Jalil, D.T.C. Nguyen, T.M. Nguyen, M. Alhassan, W. Nabgan, S. Rajendran, M.L. Firmansyah, Novel ZIF-67-derived Co@CNTs nanocomposites as effective adsorbents for removal of tetracycline and sulfadiazine antibiotics, Environmental Research 225 (2023) 115516. https://doi.org/10.1016/j.envres.2023.115516.
[18] M. Cui, Z. Che, Y. Gong, T. Li, W. Hu, S. Wang, A graphdiyne-based protein molecularly imprinted biosensor for highly sensitive human C-reactive protein detection in human serum, Chemical Engineering Journal 431 (2022) 133455. https://doi.org/10.1016/j.cej.2021.133455.
[19] E. Koudelková, Y. Ghrib, F.S. de Oliveira Ramos, P. Čičmanec, R. Bulánek, Adsorption and separation of the C3 hydrocarbons on cationic FER zeolites: Effect of dual sites existence, Microporous and Mesoporous Materials 279 (2019) 416-422. https://doi.org/10.1016/j.micromeso.2019.01.032.
[20] F. Xu, J. Yuan, C. Niu, H. Liu, D. Li, Mpg-C3N4-ZIF-8 composites for the degradation of tetracycline hydrochloride using visible light, Water Science and Technology 80(11) (2019) 2206-2217. https://doi.org/10.2166/wst.2020.038.
[21] S. Sun, Z. Yang, J. Cao, Y. Wang, W. Xiong, Copper-doped ZIF-8 with high adsorption performance for removal of tetracycline from aqueous solution, Journal of Solid State Chemistry 285 (2020) 121219. https://doi.org/10.1016/j.jssc.2020.121219.
[22] E. Zafeiraki, W.A. Gebbink, R.L.A.P. Hoogenboom, M. Kotterman, C. Kwadijk, E. Dassenakis, S.P.J. van Leeuwen, Occurrence of perfluoroalkyl substances (PFASs) in a large number of wild and farmed aquatic animals collected in the Netherlands, Chemosphere 232 (2019) 415-423. https://doi.org/10.1016/j.chemosphere.2019.05.200.
[23] S. Iravani, E.N. Zare, A. Zarrabi, A. Khosravi, P. Makvandi, MXene/zeolitic imidazolate framework (ZIF) composites: A perspective on their emerging applications, FlatChem 44 (2024) 100631. https://doi.org/10.1016/j.flatc.2024.100631.
[24] Z. Wu, X. Wang, J. Qiu, C. Liu, Z. Yu, J. Zhang, Z. Qiu, In-situ uniform growth of ZIF-8 on 3D flower-like NiCoLDH microspheres to enhance tetracycline and doxycycline removal from wastewater: Anti-interference and stability tests, Separation and Purification Technology 302 (2022) 122078. https://doi.org/10.1016/j.seppur.2022.122078.

[25] S. Keshavarz, O.V. Okoro, M. Hamidi, H. Derakhshankhah, M. Azizi, S. Mohammad Nabav1i, S. Gholizadeh, S.M. Amini, A. Shavandi, R. Luque, H. Samadian, Synthesis, surface modifications, and biomedical applications of carbon nanofibers: Electrospun vs vapor-grown carbon nanofibers, Coordination Chemistry Reviews 472 (2022) 214770. https://doi.org/10.1016/j.ccr.2022.214770.
[26] H. Wang, L. Song, L. Yu, X. Xia, Y. Bao, M. Lourenco, K. Homewood, Y. Gao, Charge transfer between Ti4+, Sn4+ and Pt in the tin doped TiO2 photocatalyst for elevating the hydrogen production efficiency, Applied Surface Science 581 (2022) 152202. https://doi.org/10.1016/j.apsusc.2021.152202.
[27] M. He, P. Zhao, R. Duan, S. Xu, G. Cheng, M. Li, S. Ma, Insights on the electron transfer pathway of phenolic pollutant degradation by endogenous N-doped carbonaceous materials and peroxymonosulfate system, Journal of Hazardous Materials 424 (2022) 127568. https://doi.org/10.1016/j.jhazmat.2021.127568.
[28] R. Wang, C. Yao, C. Peng, J. Qiu, Q. Wang, X. Liu, J. Meng, W. Wang, Ultra-strong adsorption of organic dyes and antibiotic onto the alk-MXene/ZIF adsorbents with a specific intercalation structure, Chemical Engineering Journal 485 (2024) 149916. https://doi.org/10.1016/j.cej.2024.149916.
[29] J. Yue, Q. Zheng, S. Ding, Y. Yin, X. Zhang, L. Wang, Y. Gu, J. Li, Y. Zhang, Y. Shi, Y. Dong, Q. Zhu, H. Duo, Cu–Co bimetallic organic framework as effective adsorbents for enhanced adsorptive removal of tetracycline antibiotics, Scientific Reports 14(1) (2024). https://doi.org/10.1038/s41598-024-67986-8.
[30] M. Naguib, M. Kurtoglu, V. Presser, J. Lu, J. Niu, M. Heon, L. Hultman, Y. Gogotsi, M.W. Barsoum, Two-Dimensional Nanocrystals Produced by Exfoliation of Ti3AlC2, Advanced Materials 23(37) (2011) 4248-4253. https://doi.org/10.1002/adma.201102306.
[31] D. Wang, Y. Lian, Q. Zhou, H. Fu, Y. Hu, J. Zhao, H. Zhang, An intercalated structure MXene@CCNS: cuttlefish ink-derived carbon nanospheres composite Ti3C2Tx MXene for supercapacitors, Chemical Engineering Journal 522 (2025) 167612. https://doi.org/10.1016/j.cej.2025.167612.
[32] D.-x. Sun, T. Gu, X.-d. Qi, J.-h. Yang, Y.-z. Lei, Y. Wang, Highly-toughened biodegradable poly(L-lactic acid) composites with heat resistance and mechanical-damage-healing ability by adding poly(butylene adipate-co-butylene terephthalate) and carbon nanofibers, Chemical Engineering Journal 424 (2021) 130558. https://doi.org/10.1016/j.cej.2021.130558.
[33] Z. Zhang, Y. Chen, C. Hu, C. Zuo, P. Wang, W. Chen, T. Ao, Efficient removal of tetracycline by a hierarchically porous ZIF-8 metal organic framework, Environmental Research 198 (2021) 111254. https://doi.org/10.1016/j.envres.2021.111254.
[34] J.A. Amelse, On the mechanism for ethyl transfer and removal from ethylbenzene during commercial xylene isomerization, Microporous and Mesoporous Materials 278 (2019) 275-279. https://doi.org/10.1016/j.micromeso.2018.12.005.
[35] J. Zeng, Z. Yan, D. Wang, T. He, Z. Tong, J. Miao, J. Li, W. Tan, S. Chen, Y. Deng, Mitochondria-targeted MXene@MnO2-TPP nanoheterostructures for synergistic enhancement of sonodynamic therapy and immunotherapy in osteosarcoma, Bioactive Materials 54 (2025) 450-465. https://doi.org/10.1016/j.bioactmat.2025.08.029.
[36] K. Kuśmierek, W. Kiciński, M. Norek, M. Polański, B. Budner, Oxidative and adsorptive removal of chlorophenols over Fe-, N- and S-multi-doped carbon xerogels, Journal of Environmental Chemical Engineering 9(4) (2021) 105568. https://doi.org/10.1016/j.jece.2021.105568.

[37] F. Esmaeili, G. Mazloom, J. Abdi, Y. Yoon, Novel Ti3C2Tx-MXene-embedded, leaf-like ZIF-8 polymeric beads for efficient tetracycline adsorption in batch and continuous systems, Journal of Industrial and Engineering Chemistry 148 (2025) 391-406. https://doi.org/10.1016/j.jiec.2024.12.071.
[38] D.O. Wasik, A. Martín-Calvo, J.J. Gutiérrez-Sevillano, D. Dubbeldam, T.J.H. Vlugt, S. Calero, Enhancement of formic acid production from carbon dioxide hydrogenation using metal-organic frameworks: Monte Carlo simulation study, Chemical Engineering Journal 467 (2023) 143432. https://doi.org/10.1016/j.cej.2023.143432.
[39] A. Alaei, M. Hosseini, F. Nemati, H. Karimi-Maleh, The synthesis of Pt doped WO3 nanosheets and application on colorimetric detection of cysteine by naked eye using response surface methodology for optimization, Environmental Research 212 (2022) 113246. https://doi.org/10.1016/j.envres.2022.113246.
[40] P. Lestari Handayani, T. Kim, Y. Hwa Song, J. Seo Park, S. Jae Yang, U. Hyeok Choi, Tailoring molecular interaction in heteronetwork polymer electrolytes for stretchable, high-voltage fiber supercapacitors, Chemical Engineering Journal 452 (2023) 139432. https://doi.org/10.1016/j.cej.2022.139432.
[41] S. O'Brien, E.D. Okoffo, C. Rauert, J.W. O'Brien, F. Ribeiro, S.D. Burrows, T. Toapanta, X. Wang, K.V. Thomas, Quantification of selected microplastics in Australian urban road dust, Journal of Hazardous Materials 416 (2021) 125811. https://doi.org/10.1016/j.jhazmat.2021.125811.
[42] S. Sun, A. Liu, Z. Li, T. Guo, S. Chen, G.J. Ahammed, Anthocyanin synthesis is critical for melatonin-induced chromium stress tolerance in tomato, Journal of Hazardous Materials 453 (2023) 131456. https://doi.org/10.1016/j.jhazmat.2023.131456.
[43] X. Dao, H. Hao, J. Bi, S. Sun, X. Huang, Surface Complexation Enhanced Adsorption of Tetracycline by ALK-MXene, Industrial & Engineering Chemistry Research 61(17) (2022) 6028-6036. https://doi.org/10.1021/acs.iecr.2c00037.
[44] E.Z. Afsharian, H. Sereshti, Ti2N MXene/Zn-Fe layered double hydroxide nanocomposite for efficient tetracycline removal from environmental waters: Thermodynamic and kinetic insights, Journal of Environmental Chemical Engineering 12(6) (2024) 114733. https://doi.org/10.1016/j.jece.2024.114733.
[45] C. Wang, Y. Jia, J. Li, P. Li, Y. Wang, F. Yan, M. Wu, W. Fang, F. Xu, Z. Qiu, Influence of microbial augmentation on contaminated manure composting: metal immobilization, matter transformation, and bacterial response, Journal of Hazardous Materials 441 (2023) 129762. https://doi.org/10.1016/j.jhazmat.2022.129762.
[46] Z. Jiang, M. Florian, Z. Li, K. Datta, M. Kira, P.B. Deotare, Nanoengineered Optoexcitonic Switch, ACS Nano 19(36) (2025) 32123-32130. https://doi.org/10.1021/acsnano.5c05057.
[47] M.A. Islam, M.A. Chowdhury, M.S.I. Mozumder, M.T. Uddin, Langmuir Adsorption Kinetics in Liquid Media: Interface Reaction Model, ACS Omega 6(22) (2021) 14481-14492. https://doi.org/10.1021/acsomega.1c01449.
[48] W.J. Weber, J.C. Morris, Kinetics of Adsorption on Carbon from Solution, Journal of the Sanitary Engineering Division 89(2) (1963) 31-59. https://doi.org/10.1061/JSEDAI.0000430.
[49] R. Sips, On the Structure of a Catalyst Surface, The Journal of Chemical Physics 16(5) (1948) 490-495. https://doi.org/10.1063/1.1746922.
[50] X. Chen, X. Ruan, S.E. Kentish, G. Li, T. Xu, G.Q. Chen, Production of lithium hydroxide by electrodialysis with bipolar membranes, Separation and Purification Technology 274 (2021) 119026. https://doi.org/10.1016/j.seppur.2021.119026.

[51] Y. Zou, Y. Hu, Z. Shen, L. Yao, D. Tang, S. Zhang, S. Wang, B. Hu, G. Zhao, X. Wang, Application of aluminosilicate clay mineral-based composites in photocatalysis, Journal of Environmental Sciences 115 (2022) 190-214. https://doi.org/10.1016/j.jes.2021.07.015.
[52] F. Russo, R. Castro-Muñoz, S. Santoro, F. Galiano, A. Figoli, A review on electrospun membranes for potential air filtration application, Journal of Environmental Chemical Engineering 10(5) (2022) 108452. https://doi.org/10.1016/j.jece.2022.108452.
[53] W. Shao, J. Li, Y. Zhang, N. Sun, T. Wu, M. Yan, F. Liu, H. Jiang, X. Chen, J. He, Polyvinylidene fluoride multi-scale nanofibrous membrane modified using N-halamine with high filtration efficiency and durable antibacterial properties for air filtration, Journal of Colloid and Interface Science 628 (2022) 627-636. https://doi.org/10.1016/j.jcis.2022.08.077.
[54] J. Dai, T. Chen, Q. Chen, H. Ma, X. Xu, W. Yuan, L. Wang, Facile synthesis of ZIF-8-lignosulfonate microspheres with ultra-high adsorption capacity for Congo red and tetracycline removal from water, Int J Biol Macromol 242(Pt 1) (2023) 124672. https://doi.org/10.1016/j.ijbiomac.2023.124672.
[55] M.S. Manzar, H.A. Aziz, L. Meili, I. Ihsanullah, P. Palaniandy, M.A. Al-Harthi, Insights into the adsorption of tetracycline onto cellulose nanocrystal structured MgAl/LDH composite, Materials Chemistry and Physics 299 (2023) 127247. https://doi.org/10.1016/j.matchemphys.2022.127247.
[56] R. Zhao, T. Ma, S. Zhao, H. Rong, Y. Tian, G. Zhu, Uniform and stable immobilization of metal-organic frameworks into chitosan matrix for enhanced tetracycline removal from water, Chemical Engineering Journal 382 (2020) 122893. https://doi.org/10.1016/j.cej.2019.122893.
[57] A.L. Neuer, D. Geck, A. Gogos, V.M. Kissling, A. Balfourier, I.K. Herrmann, Nanoanalytical Insights into the Stability, Intracellular Fate, and Biotransformation of Metal–Organic Frameworks, ACS Applied Materials & Interfaces 15(32) (2023) 38367-38380. https://doi.org/10.1021/acsami.3c08818.
[58] J.J. Werner, W.A. Arnold, K. McNeill, Water Hardness as a Photochemical Parameter: Tetracycline Photolysis as a Function of Calcium Concentration, Magnesium Concentration, and pH, Environmental Science & Technology 40(23) (2006) 7236-7241. https://doi.org/10.1021/es060337m.
[59] M.E. Parolo, M.J. Avena, G.R. Pettinari, M.T. Baschini, Influence of Ca2+ on tetracycline adsorption on montmorillonite, Journal of Colloid and Interface Science 368(1) (2012) 420-426. https://doi.org/10.1016/j.jcis.2011.10.079.
[60] L. van Dijk, S.P. Fletcher, Rh-catalyzed asymmetric Suzuki-Miyaura cross-coupling, Trends in Chemistry 3(9) (2021) 795-796. https://doi.org/10.1016/j.trechm.2021.05.007.
[61] H. Lgaz, H.-s. Lee, Computational investigation on interaction mechanism of sulfur mustard adsorption by zeolitic imidazolate frameworks ZIF-8 and ZIF-67: Insights from periodic and cluster DFT calculations, Journal of Molecular Liquids 344 (2021) 117705. https://doi.org/https://doi.org/10.1016/j.molliq.2021.117705.
[62] X. Deng, W. Wu, S. Tian, Y. He, S. Wang, B. Zheng, K. Xin, Z. Zhou, L. Tang, Composite adsorbents of aminated chitosan @ZIF-8 MOF for simultaneous efficient removal of Cu(II) and Congo Red: Batch experiments and DFT calculations, Chemical Engineering Journal 479 (2024) 147634. https://doi.org/https://doi.org/10.1016/j.cej.2023.147634.
[63] Q.-Q. Huang, Y.-E. Wen, H. Bai, Z. Zhang, Y. Jiang, Spontaneous Adsorption of Graphene Oxide on Multiple Polymeric Surfaces, Langmuir 37(29) (2021) 8829-8839. https://doi.org/10.1021/acs.langmuir.1c01214.
[64] P. Wu, Y. Zhao, X. Yin, H. Cao, F. Li, J. Yang, Y. Yang, N. Liu, J. Liao, T. Lan, Enhanced Photocatalytic Removal of U(VI) from Real Radioactive Wastewater by Modulating the Surface Charge

Microenvironment in Porphyrin-Based Hydrogen-Bonded Organic Framework, ACS Applied Materials & Interfaces 16(26) (2024) 33657-33668. https://doi.org/10.1021/acsami.4c06992.
[65] W. Wang, M. Qi, X. Jia, J. Jin, Q. Zhou, M. Zhang, W. Zhou, A. Li, Differential adsorption of zwitterionic PPCPs by multifunctional resins: The influence of the hydrophobicity and electrostatic potential of PPCPs, Chemosphere 241 (2020) 125023. https://doi.org/https://doi.org/10.1016/j.chemosphere.2019.125023.
[66] J. dos Santos Ferreira da Silva, D. López Malo, G. Anceski Bataglion, M. Nogueira Eberlin, C. Machado Ronconi, S. Alves Júnior, G.F. de Sá, Adsorption in a Fixed-Bed Column and Stability of the Antibiotic Oxytetracycline Supported on Zn(II)-[2-Methylimidazolate] Frameworks in Aqueous Media, PLOS ONE 10(6) (2015) e0128436. https://doi.org/10.1371/journal.pone.0128436.

Supplementary Files

This is a list of supplementary files associated with this preprint. Click to download.

- Supportinginformation20261016.docx